THE ASTROPHYSICAL JOURNAL, 502:932–943, 1998 August 1

THE SPECTRUM OF THE BROWN DWARF GLIESE 229B

B. R. OPPENHEIMER, S. R. KULKARNI, AND K. MATTHEWS
Palomar Observatory, 105-24, California Institute of Technology, Pasadena, CA 91125; bro@astro.caltech.edu
AND
M. H. VAN KERKWIJK
Institute of Astronomy, University of Cambridge, Madingly Road, Cambridge, CB3 0HA, UK
Received 1997 September 17; accepted 1998 March 9

ABSTRACT

We present a spectrum of the cool ($T_{\rm eff} = 900$ K) brown dwarf Gliese 229B. This spectrum, with a relatively high signal-to-noise ratio per spectral resolution element ($\gtrsim 30$), spans the wavelength range from 0.837 μm to 5.0 μm. We identify a total of four different major methane absorption features, including the fundamental band at 3.3 μm, at least four steam bands, and two neutral cesium features. We confirm the recent detection of carbon monoxide (CO) in excess of what is predicted by thermochemical equilibrium calculations. Carbon is primarily involved in a chemical balance between methane and CO at the temperatures and pressures present in the outer parts of a brown dwarf. At lower temperatures, the balance favors methane, while in the deeper, hotter regions, the reaction reverses to convert methane into CO. The presence of CO in the observable part of the atmosphere is therefore a sensitive indicator of vertical flows. The high signal-to-noise ratio in the 1 μm to 2.5 μm region permits us to place constraints on the quantity of dust in the atmosphere of the brown dwarf. We are unable to reconcile the observed spectrum with synthetic spectra that include the presences of dust. The presence of CO but lack of dust may be a clue to the location of the boundaries of the outer convective region of the atmosphere: The lack of dust may mean that it is not being conveyed into the photosphere by convection, or that it exists in patchy clouds. If the dust is not in clouds, but rather sits below the outer convective region, we estimate that the boundary between outer convective and inner radiative layers is between 1250 K and 1600 K, in agreement with recent models.

Subject headings: circumstellar matter — line: identification — stars: individual (Gliese 229B) — stars: low-mass, brown dwarfs

1. INTRODUCTION

Gliese 229B is the first substellar object outside the solar system with an effective temperature ($T_{\rm eff}$) well below 1800 K, the minimum $T_{\rm eff}$ for stars, to be found using direct imaging techniques (Nakajima et al. 1995). Other substellar companions have been inferred to exist through indirect techniques (Wolszczan & Frail 1992; Mayor & Queloz 1997; Butler et al. 1997). The astrophysical nature of all these objects can only be understood in detail through spectroscopic studies. Unfortunately, current technology precludes the spectroscopic study of any of these objects except Gliese 229B. Interestingly, the spectrum of a gaseous, substellar object is primarily determined by its effective temperature, and secondarily by its surface gravity and composition (Burrows et al. 1997, 1996). Thus, the spectrum of Gliese 229B is expected to resemble the spectra of some of the less massive, but similarly hot, giant planets found in the radial velocity studies.

Here we present the spectrum of Gliese 229B with a high signal-to-noise ratio from 0.837 μm out to 5 μm. Gliese 229B emits approximately 65% of its emergent flux in this wavelength region. An effort like this can perhaps be seen as a precursor to extrasolar planet studies or an extension of the work of hundreds of planetary scientists who have studied and modeled the atmospheres of the planets orbiting the Sun. In addition, these observations also give extremely interesting insights into the atmospheric physics of brown dwarfs, including the atmospheric dynamics. Our now detailed set of observations can be compared with recent models.

2. OBSERVATIONS AND DATA REDUCTION

All observations reported here were made at the Keck Telescopes. At these telescopes, a major problem in observing Gliese 229B is the presence of diffraction spikes from Gliese 229A. The image of a star produced by one of the Keck telescopes has six diffraction spikes spaced every 60° around the center of the image. These spikes are produced by both the secondary support vanes and the primary mirror's segment gaps. The spikes are fixed with respect to the horizon. In celestial coordinates, the position angle of any spike is the paralactic angle plus an integer multiple of 60° (see Fig. 1, *top panel*, *right*). As a result, the spikes rotate as the star transits the sky. Useful spectra of Gliese 229B could only be obtained when the diffraction spikes of the very much brighter Gliese 229A were $\gtrsim 15°$ away from the position angle of Gliese 229B. This reduced the time during which it was possible to observe Gliese 229B to 1.5 hr just after transit. Since Gliese 229B is not visible on the slit-viewing camera, we set up on Gliese 229A and applied a blind offset from there (7.″78 at position angle 161.°3; Golimowski et al. 1998).

2.1. *Optical Data*

We observed Gliese 229B using the Keck I telescope on 1996 January 21 (UT) with the Low Resolution Imaging Spectrometer (LRIS; Oke et al. 1995). We made three exposures of 1800 s duration each, using a Tektronix 2048 × 2048 pixel CCD with 24 μm pixels. We used the 1200 line mm^{-1} grating, blazed at 750 nm to cover the wavelength region of 847 to 973 nm at 0.06 nm per pixel. A

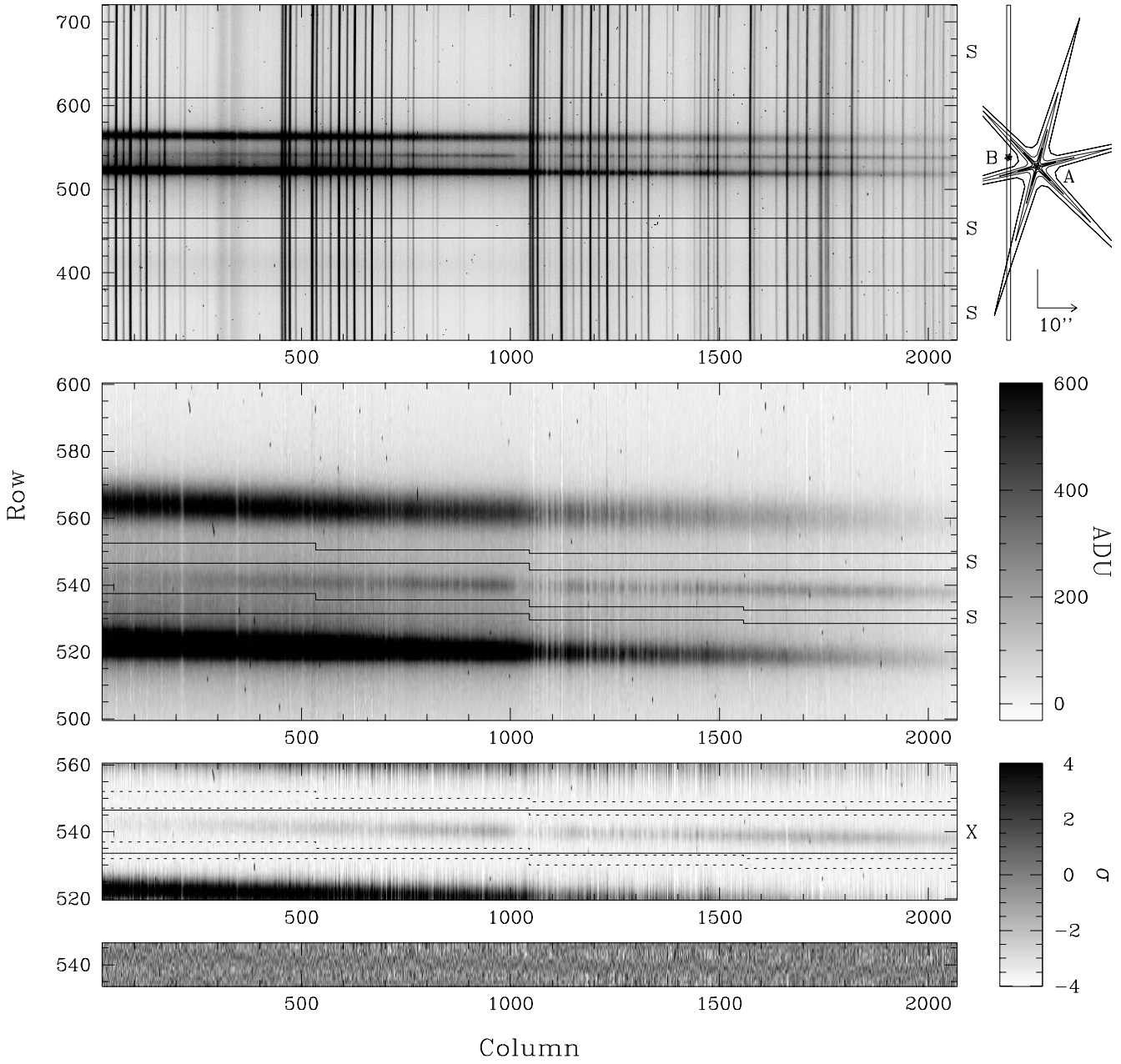

FIG. 1.—Reduction of the optical spectra. *Top panel*: One of the spectral images (a 900 s integration), after only bias subtraction and division by a normalized flat field. The whole spectral range is shown (blue to the left, red to the right), but not the full length of the slit. The grey scale is linear between −30 and 600 ADU (the gain is 2.2 e^- ADU^{-1}). A schematic view of the slit region of the spectrograph is also shown, with Gliese 229B in the slit, and 229A nearby with six diffraction spikes. Spectra of three of the spikes can be seen in the image. *Second panel*: Data after removing telluric sky emission, as determined by fitting third-degree polynomials at every column in the regions marked S at the right of the top panel. The contribution of scattered and diffracted light of Gliese 229A at the position of 229B was determined by fitting second-degree polynomials at every column in the two small regions marked S at the right of the second panel. *Third panel*: Corrected data. The absorption due to steam bands, near column 1000, is clearly seen. The spectrum was extracted from the region indicated by the two solid lines marked X at the right-hand side. Fluxes weighted according to a spatial profile (see text) are used to extract the data. *Bottom panel*: Residual after extracting the data, in units of standard deviations, to show that the extraction is accurate. The scale in the *y*-direction is the same as that in the third panel. The grey scale is linear between $-4\,\sigma$ and $4\,\sigma$, as indicated.

1″ slit, corresponding to 4.65 pixels, gave a spectral resolution of about 0.3 nm. The slit was placed east-west for all the LRIS observations. An OG570 filter suppressed the second-order spectrum.

On 1997 February 6 (UT), three more 900 s LRIS exposures were taken in the middle of the interval when the diffraction spikes were more than 15° away. The set-up was the same, except that the instrument had been moved to Keck II, and we used a new, more efficient 831 line mm^{-1} grating, blazed for a wavelength of 810 nm, covering the wavelength range 837 to 1024 nm at 0.09 nm per pixel. With the 1″ slit, the resolution was about 0.4 nm. On both nights the seeing was generally subarcsecond (∼0.″8), and a few thin cirrus clouds sailed about in the sky. The spectra from these two observations were combined by smoothing the higher resolution spectrum to the 0.4 nm resolution and adding them. Full details of the reduction technique follow.

The spectral data were reduced using MIDAS and programs running in the MIDAS environment. The presence of Gliese 229A's diffraction spikes in the spectral images

required special care during the reduction. The approach we used is illustrated in Figure 1. The top panel shows a typical spectral image, after bias subtraction and flat-field correction. First we removed the telluric emission lines (mostly OH). For this purpose, a third-degree polynomial was fitted through every column in regions free of stellar light (indicated by S on the right-hand side of the panel).

The subtraction of the strongest sky lines is not always satisfactory (see Fig. 1, *second panel*). Most likely, this results from the fact that interference fringing in the CCD is not corrected adequately for the sky emission lines, as the response of a given pixel to monochromatic light is different from the response to the continuum emission from the flat-field lamp. The resulting structure over a column has a relatively large scale, however, and is mostly removed in the next step, in which the scattered and diffracted light from Gliese 229A is subtracted by fitting a second-degree polynomial to two small regions adjacent to the spectrum of Gliese 229B (see Fig. 1). As the spectra are not aligned perfectly, these regions are chosen slightly differently for different parts of the chip.

One-dimensional spectra were extracted using a scheme similar to the "optimal extraction" technique of Horne (1986), in which an average stellar profile along the slit is created to estimate the total flux from each pixel in a given column. All estimates are combined using weights inversely proportional to the square of each pixel's formal uncertainty (determined from the read noise and Poisson noise in the raw data). In the third panel of Figure 1, we show the difference between the raw data and the extracted data (in standard deviations). It is apparent that the extraction is quite accurate, since very little structure remains. We also extracted the spectrum of Gliese 229A with the same technique, after removing the contribution from Gliese 229B from the image. This allows us to verify that no contamination from Gliese 229A remains in Gliese 229B's spectrum. Indeed, Figure 6 shows that none of the features in A are present in the spectrum of B.

Wavelength calibration employed argon and krypton/mercury arc spectra taken after the series of exposures. For the 1200 line mm^{-1} spectra, only 7 lines were available, but they were quite evenly spread over the wavelength range. A fit to the positions of these lines with a third-degree polynomial left a root mean square residual of 0.023 pixel. For the 831 line mm^{-1} spectra, 11 lines were used (achieving an rms of 0.03 pixel), but none of these were longward of 970 nm. However, a comparison of the locations of OH airglow lines in our spectral images with the wavelengths given by Osterbrock, Fullbright, & Bida (1997) shows that the wavelength calibration is accurate to better than 0.1 nm everywhere on the spectrum. For removal of telluric water vapor lines as well as relative flux calibration, we used spectra of Feige 34 (sdO; $V = 11.2$; Massey & Gronwall 1990), taken after Gliese 229B at similar air mass. The final absolute flux calibration was achieved using the photometric results from Matthews et al. (1996).

2.2. *Infrared Data*

On the nights of 1997 February 8 and 9 (UT), we obtained the *Z*, *J*, *H*, *K*, *L*, and *M* band spectra using the Near Infrared Camera (NIRC; Matthews & Soifer 1994) at the Cassegrain focus of the Keck I telescope. These spectra were obtained in several stages using the grism mode of the camera. The camera permits recording of low-resolution spectra in the *Z*, *J*, and *H* bands simultaneously, then the *H* and *K* bands, and finally the *L* and *M* bands. The *ZJH* region was obtained in 10 exposures of 40 s of on-source exposure time. After every 40 s exposure, we shifted the telescope 15".6 north and took a 40 s long sky frame. The slit was placed east-west, as it was during the LRIS observations. This produced pairs of on-source exposures taken right before corresponding sky exposures. The distance 15".6 was chosen so that we would be sampling exactly the same sky background relative to the primary star (Gliese 229A), but on the opposite side of the star. This seemed to be the optimal way to remove the point-symmetric background.

We used the grism with 150 line mm^{-1} and a slit 4.5 pixels wide (0".675) to obtain the *ZJH* spectrum. Blocking filters were in place so that only light from the *Z*, *J*, and *H* bands reached the detector. The *H*-band spectrum was obtained a second time in a series of 22 more 40 s exposures (plus 22 corresponding sky exposures) in which the *H* and *K* spectra were recorded. In these spectra, the 120 line mm^{-1} grism was in place with corresponding blocking filters as well. The weather was clear and photometric and the seeing was 0".7 on both nights.

The *L*- and *M*-band spectra were slightly trickier to obtain. As far as we know, this work represents the first time the Keck telescope has been used for 3 μm to 5 μm spectroscopic observations. As a result, we had to ascertain which electronics settings were optimal and what readout times and integrations were necessary. As shown by the results presented here, NIRC is fully capable and rather sensitive in these wavelength bands.

All the spectral images contained both Gliese 229A and 229B, because of the diffraction spikes of A. Data reduction involved the following steps. For each on-source frame (which entailed the coaddition by the NIRC electronics of 1000 individual array readouts), we subtracted the sky frame immediately following. We then extracted spectra from bars ten pixels in width across the slit of both Gliese 229B and 229A. Gliese 229B's spectral signature was quite detectable in the single sky-subtracted images. The extraction technique involved the optimal extraction method, in which the pixels are summed in the spatial direction but weighted according to the signal in each pixel. The technique is similar to that used for the optical data, and it leads to a significant improvement in signal-to-noise ratio over simple addition. To make sure that the sky background and particularly any contamination from 229A were not present in our final spectrum, we subtracted the corresponding optimally extracted spectrum ten pixels to either side of the spectral region of 229B.

We removed the instrumental response by dividing the extracted spectrum by the extracted spectrum of a calibrator star. For the *Z*, *J*, *H*, and *K* bands, this calibrator was SAO 175039, a G8 star that smoothly approximates a blackbody spectrum through this wavelength region, except for a few hydrogen absorption lines, which we edited out by linear interpolation. For the *L* and *M* bands, we used Gliese 229A, an M1 V star that is quite flat in the region redward of 2 μm. (For *L* and *M* spectra of other early M dwarfs, see Berriman & Reid 1987 or Tinney, Mould, & Reid 1993.) Ideally, one should use a calibrator star such as a bright F- or G-type star. However, the use of 229A is sufficient in this case. Absolute flux calibration involved matching the flux density in the spectrum with the photometric measurements of Matthews et al. (1996).

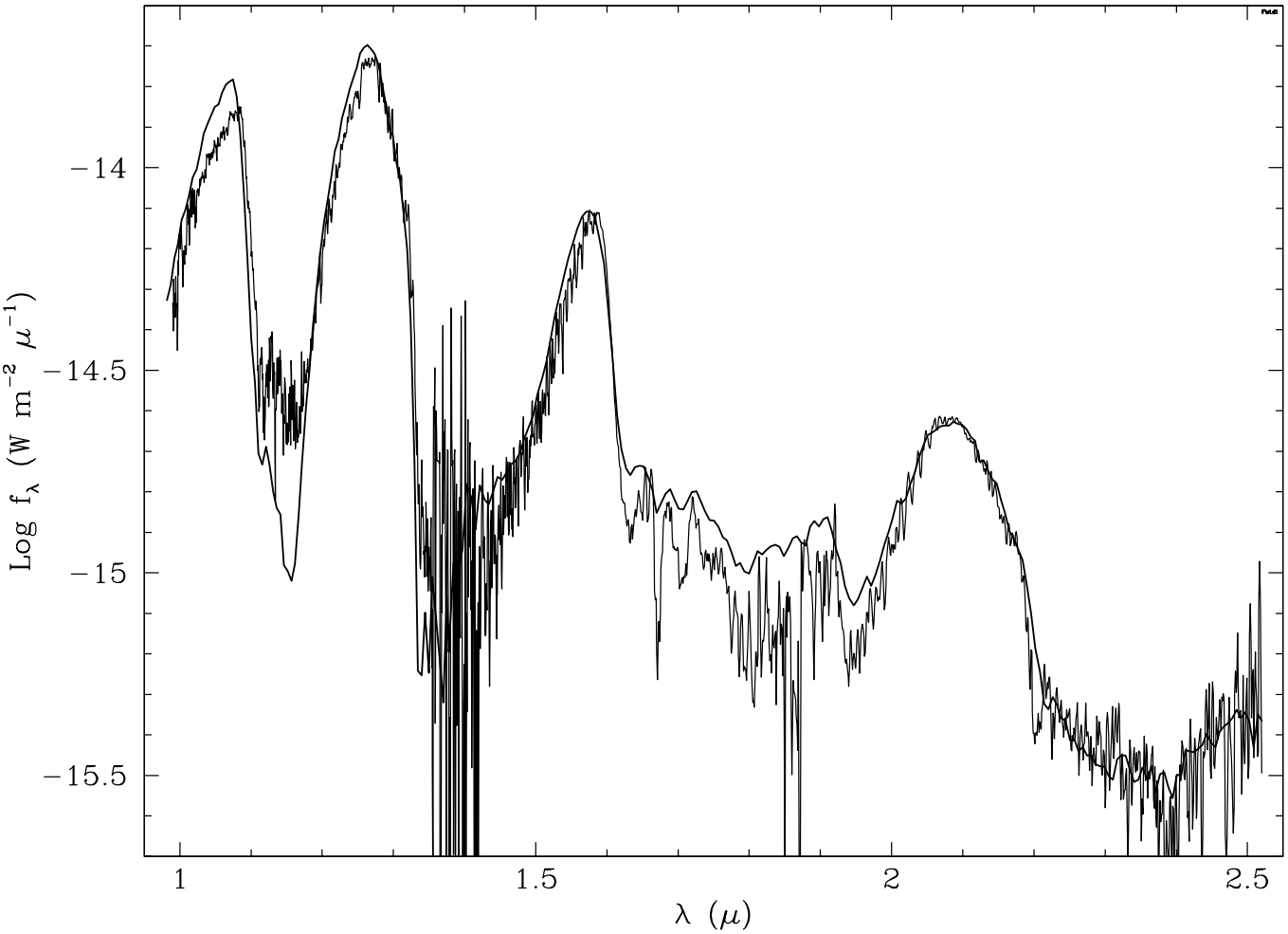

FIG. 2.—Keck NIRC spectrum of Gliese 229B (*thick line*) compared with the UKIRT CGS4 spectrum (*thinner line*, higher resolution). The agreement between the two spectra is good except in the 1.6 to 2 μm region and the 1 to 1.1 μm region. The discrepancies are, however, no more than 10% of the signal, and are most likely due to small differences in wavelength calibration and possibly to atmospheric dispersion, which could put some of the flux at the blue end of the UKIRT spectrum just outside the slit. This would explain the fact that the discrepancies are mostly at the blue end of the spectrum. Alternatively, there may be minor residual contamination from Gliese 229A in our spectrum. The UKIRT spectrum is taken from Geballe et al. (1996).

The wavelength calibration of the infrared data involved a simple method. We used the edges of the filter bands, clearly visible in the calibrator star spectra, to determine the wavelengths of the edges of each segment of the spectrum. The 50% transmission points of the bands are known to an accuracy of 10 nm. With these "edge wavelengths" known, we linearly interpolated to determine the wavelength for each pixel across the spectrum. This introduces errors on the scale of 1 nm.

Finally, we added all of the extracted, calibrated spectra together.

Figure 2 compares our 1–2.5 μm spectrum with the higher resolution spectrum of Geballe et al. (1996). The plot shows that there is good agreement between the spectra. The differences, which are most pronounced in the 1–1.1 μm and 1.6–2 μm regions, amount to no more than 10% of the signal. These discrepancies may be due to possible minor contamination from Gliese 229A in the 1.6–2.0 μm region of our spectrum as well as some minor differences in wavelength calibration. Alternatively, the Geballe et al. (1996) spectrum might have been affected by atmospheric dispersion, causing some of the bluer wavelengths to be slightly reduced in brightness, since some of the blue light would have been blocked by the slit. In Geballe et al. (1996), it is shown that the small features in the brighter parts of the spectrum are almost entirely real and correspond closely to known absorption lines in water. Our spectrum is unable to resolve these features. However, the agreement between the spectra is an excellent confirmation of the data, as well as an indicator that our reduction method works and has no major contamination from scattered light from Gliese 229A.

Figure 3 shows the relative instrumental response of NIRC with the 60 line mm^{-1} grism in the L band plotted along with our spectrum of Gliese 229B. The absorption band at about 3.4 μm is due to the resin inside NIRC. This resin is applied to the surface that will become the grating. Then a master grating is pressed against the resin so that an imprint of the grating is left in the resin, which subsequently dries and becomes the "replicant" grating used in NIRC. The instrumental transmission curve is simply the extracted spectrum of Gliese 229A, which, as we mentioned above, is flat in this region. The final spectrum of B shows none of the features attributed to this instrumental response.

3. THE SPECTRUM

The complete spectrum is presented in Figure 4, with the

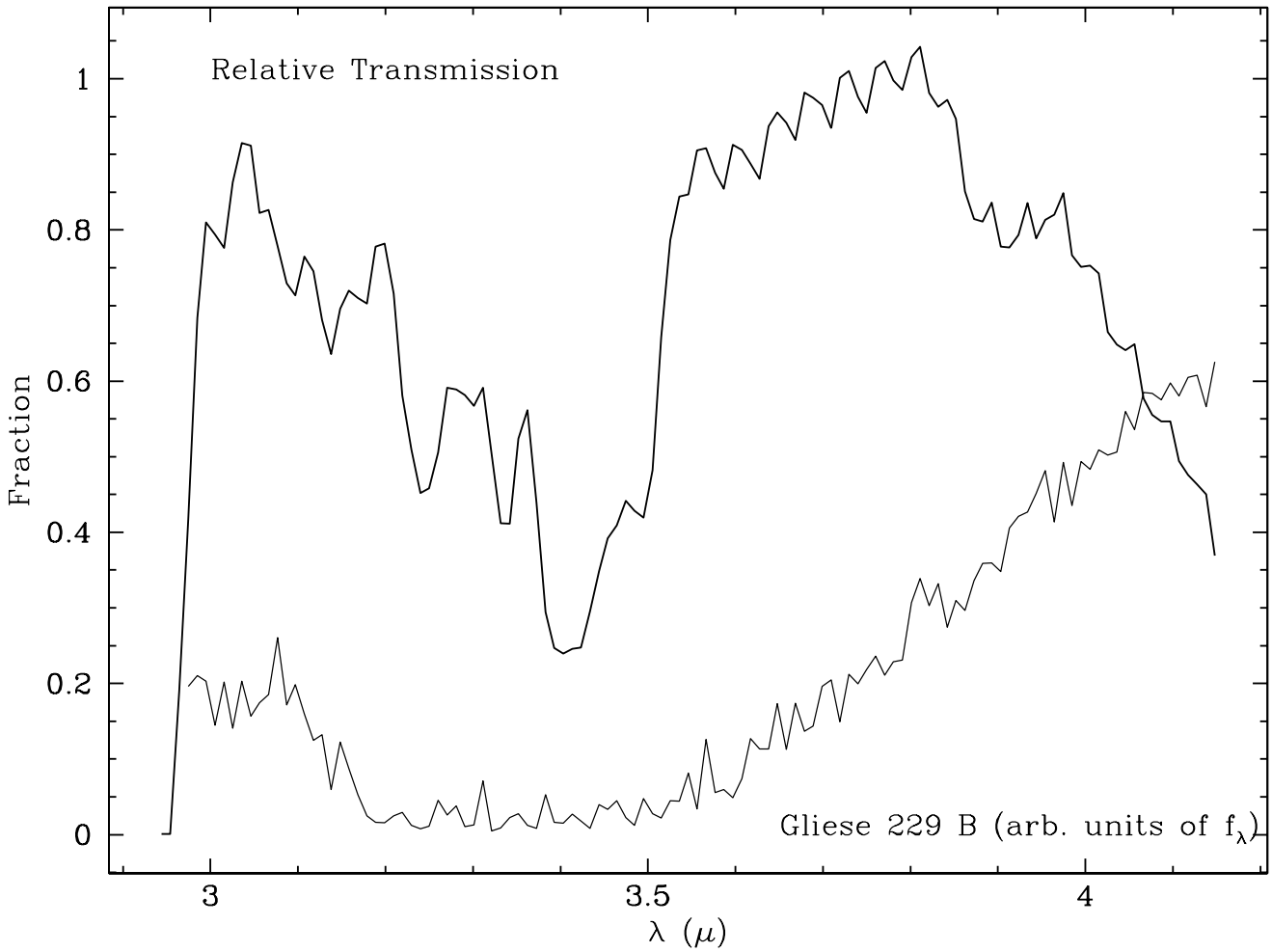

FIG. 3.—Relative instrumental transmission of NIRC through the L band (*heavy line*) and the f_λ of Gliese 229B (*lighter line*). The large variations in the instrumental transmission are produced by the resin that forms the rulings on the grism in NIRC. See § 2.2 for a more detailed discussion.

most important features labeled. The 1–2.5 μm part of this spectrum has been discussed in detail in Oppenheimer et al. (1995) and Geballe et al. (1996). Here we concentrate on the new short- and long-wavelength parts. In the latter, we find the fundamental methane band at 3.3 μm and an interesting small feature in the M band that we attribute to CO, in confirmation of the claims of Noll, Geballe, & Marley (1997; see § 6). In the optical part, shown enlarged in Figure 5, there are two prominent atomic lines from cesium, a very weak feature caused by methane, and a strong steam band. These are all discussed in detail in the following sections.

Before discussing the detailed parts of the spectrum, it is useful to compare the spectrum of Gliese 229B with spectra of some of the lowest mass stars. Figure 6 shows the optical part of the spectrum compared with that of vB 10 and LP 944−20, which were studied by Kirkpatrick, Henry, & Irwin (1997). Note the distinct absence in Gliese 229B of any of the molecular absorption features arising from refractory elements, such as VO and TiO. In addition, the steam feature is far deeper and more exaggerated in Gliese 229B. In contrast to the stars, Gliese 229B seems smooth blueward of the steam feature, with the exception of the two neutral cesium lines and a possible faint methane feature. (See § 8 and § 4 for a detailed discussion.)

Figure 7 compares Gliese 229B's near-IR spectrum with those of GD 165B and vB 10 again. The comparison spectra are reproduced here courtesy of H. R. A. Jones and appeared in Jones et al. (1994). The huge swings in flux density in Gliese 229B are not to be found in either star. In particular, this figure shows the great importance that methane has in Gliese 229B's spectrum, causing drastic drops in the flux density at 1.6 μm and 2.2 μm.

The water bands at 1.1 μm and 1.4 μm are also vastly deeper in Gliese 229B than in the stars. More specifically, the water band at 1.4 μm is about 2.5 times deeper in Gliese 229B than it is in GD 165B. Some of these differences may be magnified by the presence of dust in GD 165B and vB 10. Dust serves to smooth out spectra such as these, and it has recently come to light that dust is quite important in the spectra of some very low mass stars (Jones & Tsuji 1997; see also § 7.)

Interesting comparisons can be made between the Gliese 229B spectrum and that of Jupiter. Although the spectrum of Jupiter is produced by reflected sunlight throughout the wavelengths discussed here, there exist many similarities. We discuss these in the sections below where appropriate.

What follows is a detailed explanation of various aspects of Gliese 229B that can be addressed with the data presented in this paper.

4. METHANE

Our spectrum in the 3–4 μm region shows an extremely

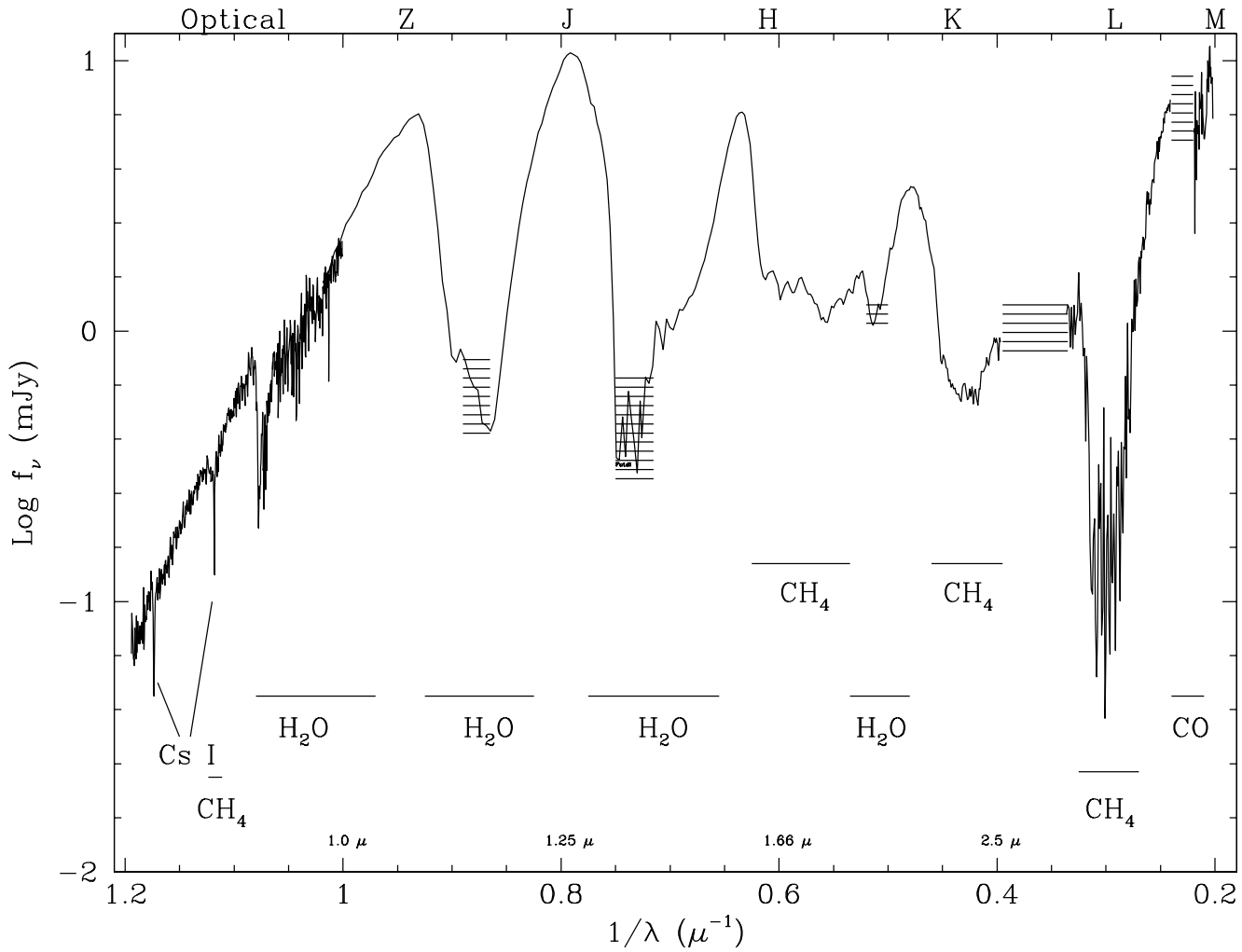

FIG. 4.—Spectrum of Gliese 229B from 0.84 to 5 μm. Major opacity sources are indicated. Regions with horizontal bars correspond to wavelengths where the atmosphere is too opaque to permit collection of useful data from the ground. Along the top of the plot are indicated the filters corresponding to the various wavelength bands.

large absorption feature (Fig. 4). We attribute this to the fundamental methane absorption band, which has been observed in planets and moons in the solar system. Noll (1993) detected an interesting spike in the spectrum of Jupiter at 3.52 μm. Other researchers have also noticed this feature (Drossart et al. 1996). We do not see this feature in our spectrum of Gliese 229B. Drossart et al. (1996) attribute this feature to reflected solar light emerging between what are actually two important methane features. The principal reason we cannot comment on the presence of this feature in Gliese 229B is that the signal-to-noise ratio in this part of the spectrum is exceedingly low. For that reason, the depth of this band cannot be determined from this data.

Another formerly undetected band of methane presented here is the faint band in the 0.89 μm region. This band, which is quite prominent in the reflectance spectra of Jupiter, Saturn, Titan, Uranus, and Neptune, has been shown by Karkoschka (1994) to be strongly dependent upon the effective temperature. Large differences in the depth of the band are apparent in the spectra he presents. This is important because the temperature dependence of the absorption coefficient for methane is poorly known. Examination of the results of Karkoschka (1994) show that this band should be extremely weak at high temperatures, such as the 900 K temperature of Gliese 229B. Thus, the weakness of this feature is expected.

5. WATER

Water is by far the most important source of noncontinuum opacity in Gliese 229B. (Continuum opacity comes, as indicated by models, from H^-, H_2^-, and H_2 collision-induced absorption; Burrows et al. 1997.) In models of Gliese 229B, the absorption between the near-IR filter bands (which are naturally defined by telluric water absorption) are broad and deep. This is highly beneficial. It means that the majority of the flux from Gliese 229B and any similar objects, such as extrasolar giant planets, will pass through the Earth's atmosphere (Matthews et al. 1996), and that brown dwarf or extrasolar planet studies are not hindered by this telluric absorption.

Geballe et al. (1996) showed that the narrow features in the 2.0–2.2 μm region correspond closely to the opacity of water. Saumon et al. (1996) have shown that a measurement of the surface gravity of Gliese 229B could be made using these very fine water features.

The optical spectrum (Fig. 5) shows many narrow features redward of 0.925 μm. These are essentially all real features and are a result of the complex structure of the

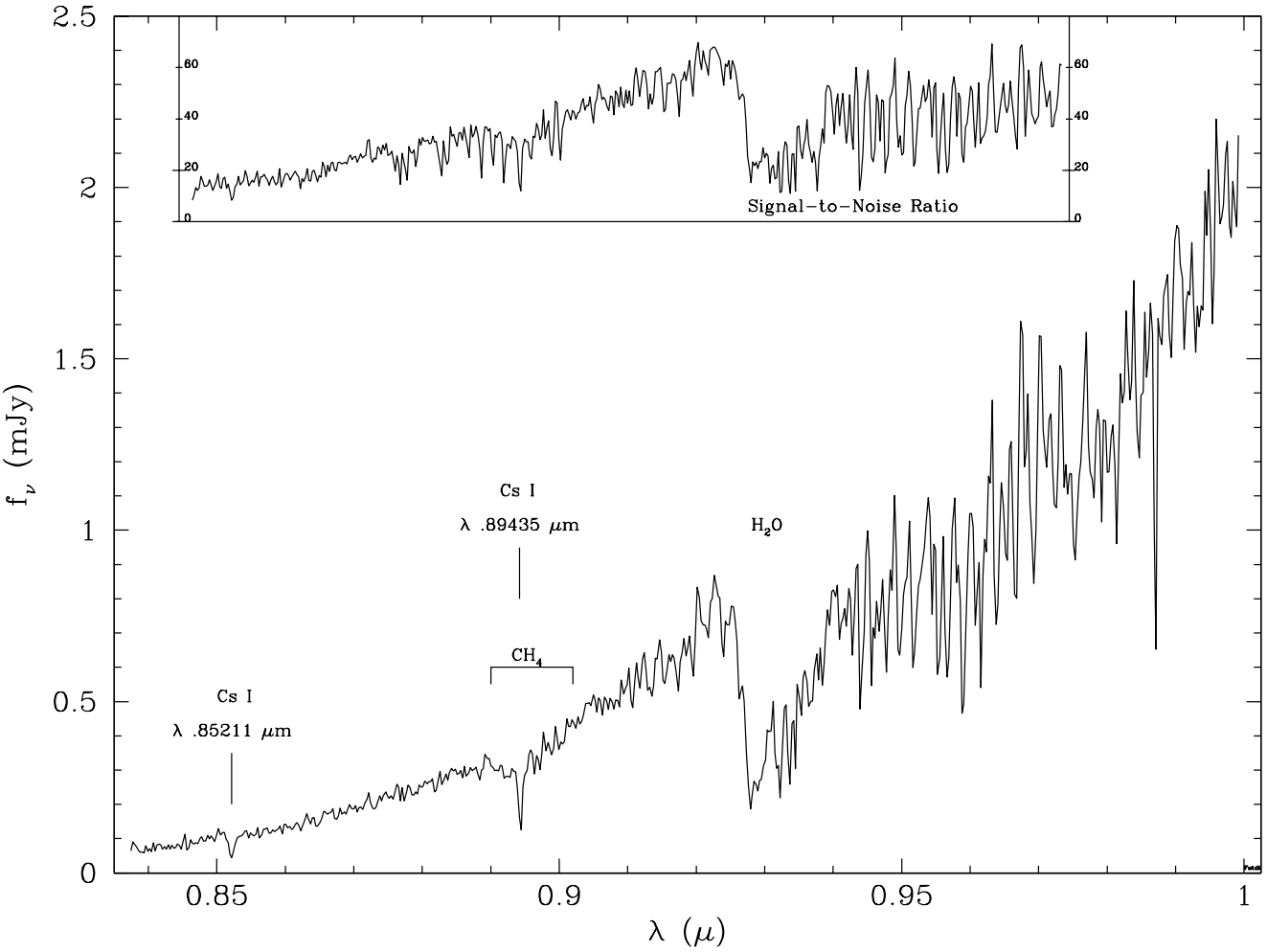

FIG. 5.—Spectrum of Gliese 229B from 0.837 to 1.0 μm. Important absorption features are labeled. The upper panel is a graph of the S/N ratio through the central region of the spectrum. The redward end of the spectrum degrades considerably in S/N ratio because of the decreasing sensitivity in the CCD. The seemingly noisy long-wavelength end of this spectrum contains what are largely real features. The dips in S/N ratio near 0.88 μm are caused by telluric emission lines.

water molecule (F. Allard 1997, private communication). In principle, one can conduct an analysis of these water features similar to that in Meadows & Crisp (1996), in which the thermal structure of the atmosphere of Venus was deduced. However, this entails modeling line profiles and spectral synthesis with detailed radiative transfer models, which our group is unable to do at present. Unfortunately, the models of Venus cannot be used because Gliese 229B (presumably) has no rocky surface underlying its atmosphere. In the case of Venus, the surface has a profound impact on the radiative processes in the atmosphere (Meadows & Crisp 1996).

6. CARBON MONOXIDE

The first vibration-rotation band (1–0) of CO is centered near 4.7 μm. Motivated by a paper by Fegley & Lodders (1996) that discussed the importance of the detection of CO, we measured the 3–5 μm spectrum of Gliese 229B presented here. Since then, the presence of CO in the atmosphere of Gliese 229B has been reported by Noll et al. (1997; hereafter NGM). NGM, using spectral data in the 4.7 μm region, claim to detect the expected increase in flux density in the center of the 1–0 vibration-rotation band. Although the noise in their data was appreciable, the detection is clear and the model spectrum they generated agrees well with the data.

Our data confirm their result, as can be seen in Figure 8, where we have reproduced NGM's Figure 2 (courtesy of Mark Marley), showing their data and model, but with our data overdrawn. Their model fits the observations best with a mole fraction, q, of $q\mathrm{CO} = 200$ ppm (parts per million) and a brown dwarf radius of 8×10^4 km (which affects the flux density as well as the model's adiabat). We have scaled the flux density of the NGM data by a factor of 2 to match the flux density we measured in Matthews et al. (1996). The uncertainty on each of the points in our data is approximately 2/3 the uncertainty in the data of NGM. Our data fit the model extremely well, even in regions where the NGM data do not.

NGM state that the sudden break at 4.82 μm in their spectrum is due to incorrect removal of a telluric line. Indeed, we do not see this feature in our spectrum.

As NGM discuss, one does not expect CO to be present in the atmosphere of Gliese 229B in thermochemical equilibrium. Fegley & Lodders (1996) computed models of the thermochemical equilibrium abundances of many molecules for a pressure-temperature profile of Gliese 229B from Marley et al. (1996). They found that only at a tem-

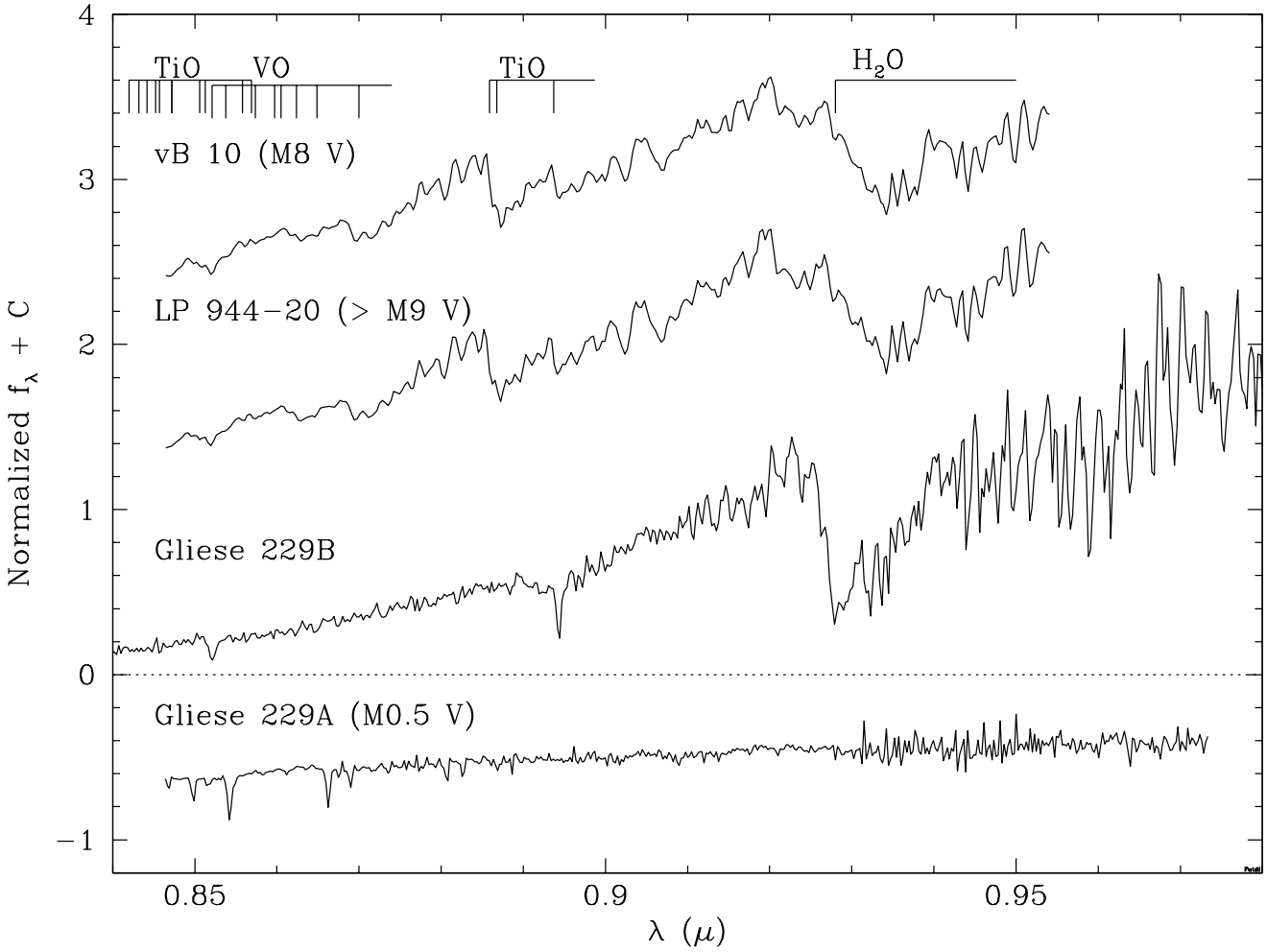

FIG. 6.—Optical spectrum of Gliese 229B compared with spectra of two of the least massive stars known, vB 10, an M8 V star, and LP 944−20, whose spectral classification is $\gtrsim$M9 V according to Kirkpatrick et al. (1997). These spectra are presented here courtesy of J. D. Kirkpatrick and appeared earlier in Kirkpatrick et al. (1997). The values of C are 1.0 for LP 944−20 and 2.0 for vB 10. Line locations, with the exception of Cs and CH_4, are from Kirkpatrick et al. (1991).

perature of about 1400 K would one expect the mole fraction of CO to equal that of CH_4. At 1250 K, CO is about 10 times less abundant. At the 900 K isotherm, one would expect the abundance of CO to be almost 10^{-4} times that of CH_4. In the atmospheres of Jupiter and Saturn, the $q\mathrm{CO}/q\mathrm{CH}_4 = 1$ boundary is much deeper (Fegley & Lodders 1994). The only explanation for the presence of CO in the photosphere of Gliese 229B is that it is not in thermochemical equilibrium. This seems to require convection, which would bring measurable quantities of CO up from the deeper and warmer parts of the atmosphere. The convection need not necessarily reach all the way to 1400 K. Even if it extended into the 1250 K region, substantial quantities of CO could be pulled up into the outer atmosphere (Fegley & Lodders 1994, 1996).

This indicates that the outer convective region of Gliese 229B is at least as deep as the 1250 K isothermal surface. Recent models by Burrows et al. (1997) found that an object like Gliese 229B has an outer radiative region, followed as one progresses inward by a thin convective region spanning a temperature range that depends upon the mass and effective temperature. Below this thin outer convective region lies another radiative region that extends in almost all the models to a depth where the temperature is about 2000 K. Inside this inner radiative region is a final convective region that reaches to the core of the brown dwarf. This concept of shells of alternating convective and radiative regions seems to be in agreement with the observations made here. The CO might form easily in the outer convective shell, which can reach temperatures of over 1250 K, and get dredged up to the observable part of the atmosphere. To make this more clear, one must consider the presence of dust in the spectrum of Gliese 229B.

7. DUST

The issue of dust in Gliese 229B has been the subject of some discussion, particularly among modelers of brown dwarf and planet atmospheres (e.g. Marley et al. 1996; Tsuji et al. 1996b; Allard et al. 1996). At some point in the near future, the application of a detailed theory of the cloud microphysics (such as appears in Rossow 1978) may be possible. For now, we restrict ourselves to a somewhat more qualitative discussion.

Metallicity of Gliese 229B is important to any discussion of its dust content. At this time we have no direct measurement of the metallicity of Gliese 229B. However, the two measurements of the metallicity of Gliese 229A are $[M/\mathrm{H}] = +0.15 \pm 0.15$ (Mould 1978) and [Fe/H] =

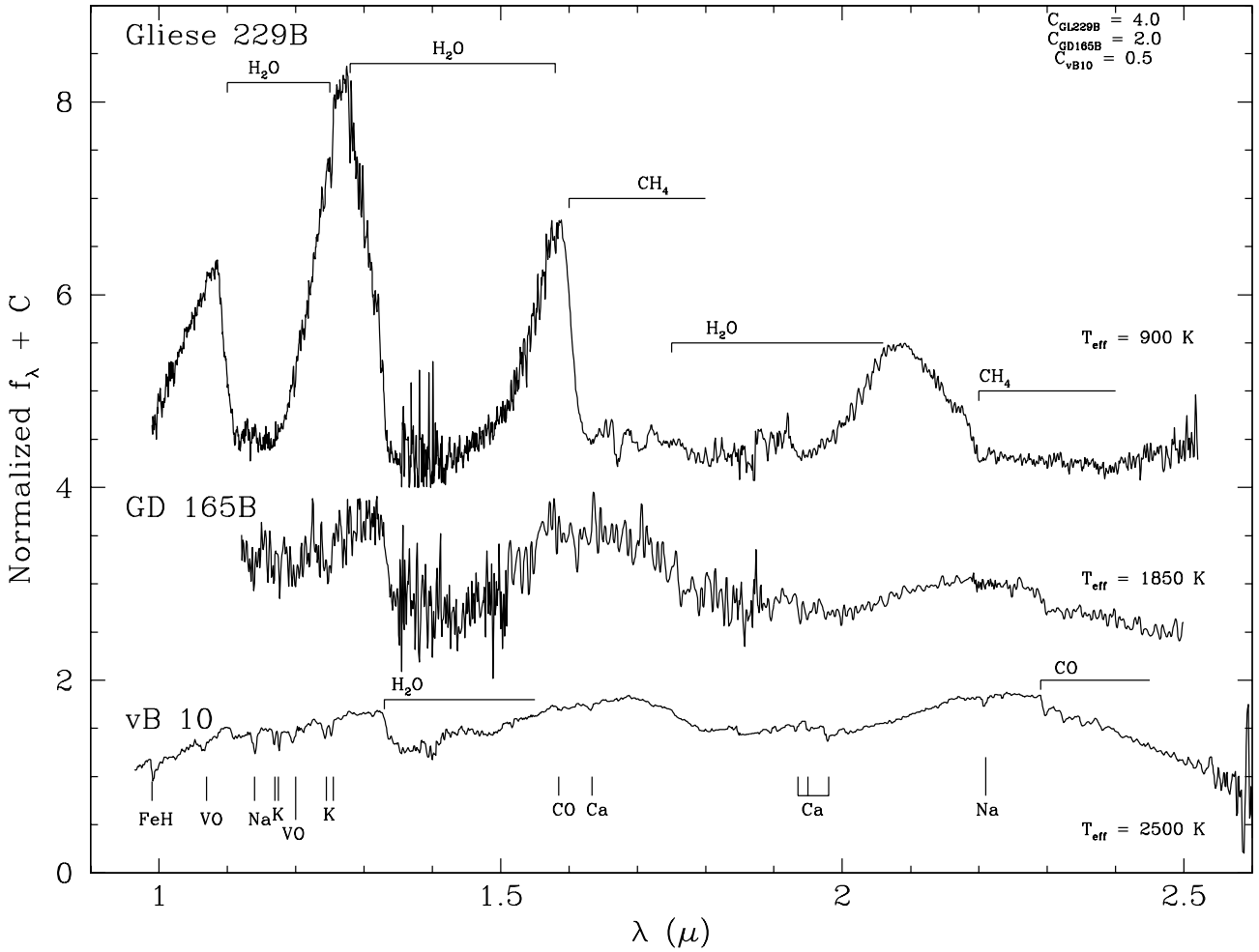

FIG. 7.—Near-IR spectrum of Gliese 229B compared with spectra of vB 10 and GD 165B. The IR spectrum is that of Geballe et al. (1996) and is used because it matches the resolution of the other two spectra, which appear courtesy of H. R. A. Jones and were first published in Jones et al. (1994). The importance of methane in the spectrum of Gliese 229B is best demonstrated in this figure. The distinct drop-off in flux density at 1.6 and 2.2 μm are features not to be found in stellar spectra. The water bands at 1.1 and 1.4 μm are also grossly magnified in strength in Gliese 229B. The absorption line identifications for vB 10 are from Jones et al. (1994).

-0.2 ± 0.4 (Schiavon, Barbuy, & Singh 1997), which are both consistent with solar metallicity (within the error bars). If Gliese 229B formed the way planets are thought to form, out of a circumstellar disk surrounding the nascent Gliese 229A, it may be that the metallicity of the brown dwarf is higher than that of its sun, as is the case for the outer planets of the solar system. In this case, one would expect to see even more dust (Burrows et al. 1997). On the other hand, if Gliese formed out of the collapse of an interstellar cloud, the way Gliese 229A presumably formed, the metallicities should be identical. This is important because of the apparent lack of dust influences in the spectrum, as we discuss below.

Jones & Tsuji (1997) have demonstrated that dust plays an extremely important role in the spectra of the very lowest mass stars. Looking at progressively cooler stars, Jones & Tsuji (1997) find that dust increases in importance past the spectral classification M6. The evidence for this is that the prominent TiO and VO bands that define late M-type spectra suddenly seem to reduce in strength past the M6.5 V spectral type. This cannot be reconciled with dust-free models of late-type stars, which show increasing strength in the TiO and VO bands until the bottom of the main sequence (Allard & Hauschildt 1995). Furthermore, Tsuji, Ohnaka, & Aoki (1996a) have shown that GD 165B's spectrum can only be explained by the presence of large quantities of dust. It may be that past the M6.5 V spectral type stars do not all appear the same; some may be rather dusty, while others may not. This might be the result of differences in metallicity and in details of the stars' weather patterns. Observational support for such differences comes from the diversity of spectra observed by Kirkpatrick et al. (1997).

The results of Jones & Tsuji (1997) would lead one to expect that a substellar object such as Gliese 229B would be even more affected by dust. However, based on the photometry of Gliese 229B (as reported by Matthews et al. 1996), Tsuji et al. (1996b) concluded that dust does not play a role in determining the spectral energy distribution. From our high signal-to-noise ratio spectral data through the deepest parts of the methane absorption bands, we can more quantitatively compare the observed spectrum with a range of spectra calculated with differing quantities of dust. We find that the spectrum presented here cannot be reconciled with any of the dusty models that Tsuji et al. (1996b) computed. Even the least dusty model of Tsuji et al. (1996b) does not fit the observed spectrum. For instance, the observed factor of

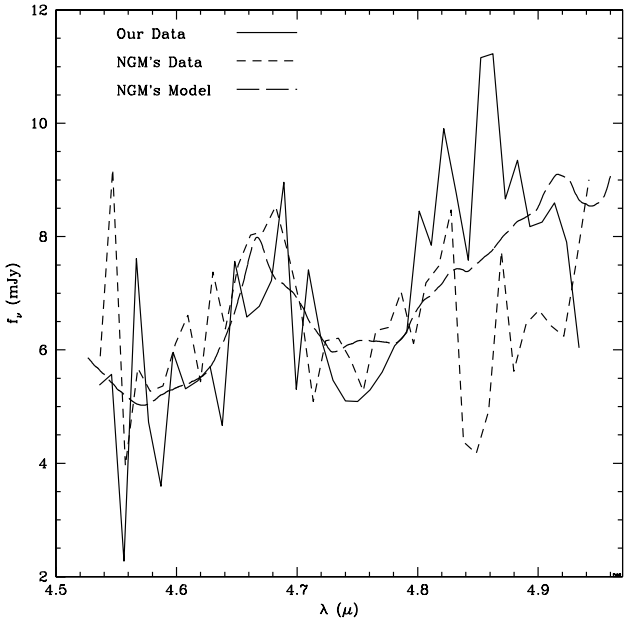

FIG. 8.—Expanded view of the spectrum of Gliese 229B between 4.5 and 5.0 μm. The solid line represents the data presented in this paper, while the short-dashed line comes from NGM, as does the model spectrum represented by the long-dashed line. Typical uncertainties in our data points are about 2/3 those of NGM, which are on the order of 2 mJy. Our data confirm the detection of carbon monoxide in Gliese 229B's atmosphere. The peak at 4.67 μm is due to a gap in the middle of the 1–0 vibration-rotation absorption band of CO. The model uses a mole fraction of qCO = 200 ppm and a brown dwarf radius of 80000 km. The feature at 4.85 μm in the NGM data is due to incorrect removal of a telluric line. Their data and model appear courtesy of K. Noll, T. Geballe, and M. Marley.

10 drop in flux density in the K band matches only the dust-free models of Tsuji et al. (1996b). The dusty models of Tsuji et al. (1996b) show a pronounced dampening of this methane absorption band.

The question that now arises is: Where is the dust that is expected to be present in the brown dwarf? We see two possibilities. The first, suggested by Tsuji et al. (1996b), is that the lack of dust is only apparent; the dust that one expects from thermochemical considerations is present, but in clouds in the photosphere with a small covering fraction. This would presumably be an observably testable suggestion. One could look for variability in the absorption bands of Gliese 229B. In the various spectral images we have taken at Keck and Palomar, we found no evidence for variability greater than 10% on timescales from several minutes to two days and over a 1 yr baseline in the 1.6 μm methane absorption band, the depths of which are easily detected in a single 40 s exposure on Keck. Whether the presence of clouds would produce a 10% or larger effect is not clear. However, this is probably a viable explanation.

Another possible explanation for the lack of dust is that it sits deep within the atmosphere below the outer convective region in an inner radiative region (first predicted in planets by Guillot et al. 1994, and predicted to exist in brown dwarfs by Burrows et al. 1997), so that it is not blown back up into the photosphere through convection. There are several points we can raise in support of this idea.

We argued above (§ 6), in confirmation of NGM, that there is an appreciable quantity of CO visible in the spectrum of Gliese 229B, and that this is many orders of magnitude higher than the amount expected from thermochemical equilibrium. We further argued that this could be the result of convection in the brown dwarf's atmosphere. This seems to imply that the convective region of the brown dwarf must extend at least to a depth where CO is abundant. Fegley & Lodders (1996) showed that the CO to CH_4 phase transition ought to happen at around 1400 K and a pressure of about 10 bars in Gliese 229B. As mentioned above, it is possible that the CO we observe comes from a lower temperature where it exists but in smaller relative quantities. Thus, it could perhaps come from as low a temperature as 1250 K, where the mole fractions of CO and CH_4 differ by a factor of 10. We already know, however, that the dust forms at much higher temperatures than this. By far the most abundant refractory elements are Fe, Mg, Si, and Al. These form Al_2O_3 (corundum) in the late M dwarf regime, Fe clusters at 2000 K (Fegley & Lodders 1996), and $MgSiO_3$ (enstatite) at 1600 K (Tsuji et al. 1996a; Sharp & Huebner 1990).

This may indicate where the boundary between the outer convective and inner radiative regions of the brown dwarf are. Specifically, the boundary must be at a temperature above 1250 K, to permit dredging of substantial quantities of CO into the cooler regions, and yet cooler than 1600 K, where enstatite forms. If the outer convective region extends deeper and hotter than 1600 K, then the condensation and falling or raining rate of enstatite must be much faster than the convective wind speed, so that the enstatite and other types of dust never reach the outer atmosphere. This process would be similar to the falling of rain droplets in the Earth's convective and stormy atmosphere. Rain falls despite the convection. Presumably one could model this process to answer the question raised in this paragraph. If the dust is below the outer convective region in a radiative region, clouds are not needed to reconcile the observations with theory.

According to Marley et al. (1996) and Marley (1997), theoretical temperature versus pressure curves for Gliese 229B show that the atmospheric structure becomes adiabatic at approximately 1600 K and 10 bars of pressure. This is consistent with our suggestion above, that the outer convective/inner radiative boundary is between 1250 K and 1600 K. It is also consistent with the new models by Burrows et al. (1997).

If this is true, then one would predict that objects at some temperature below the 1800 K of GD 165B will begin to show the effects of dust less and less. Indeed, the expectation is that the much hotter brown dwarfs will exhibit dust in their spectra. The possibly close proximity of the radiative-convective boundary in Gliese 229B to the formation temperature for enstatite suggests that a brown dwarf even slightly hotter than Gliese 229B might show some effects of dust in its spectrum. Thus, one should see a progressive decrease in the importance of dust through the range of effective temperatures from 1800 K to 900 K. Alternatively, below a certain temperature, the photosphere may become dust free. This could happen if convection is unable to bring the dust back into the photosphere because it just rains out of the convective region.

It is entirely possible, however, that the type of internal structure we discuss here is largely model dependent. For example, additional, as yet unidentified, opacity sources inside the brown dwarf atmosphere could upset or even drastically change the conclusion that there are inner radiative and convective zones.

As a final note on the dust in Gliese 229B, we remark upon the smooth-looking parts of the optical spectrum. These may be due to a haze of exotic types of dust not yet identified that have an extremely fine particle size, but this requires additional work on behalf of the modelers (M. Marley & F. Allard 1998, private communication).

8. CESIUM

Of the alkali metals (Li, Na, K, Rb, Cs, and Fr), only lithium, sodium, potassium, and rubidium have been known to play an important role in low-mass star spectra (Kirkpatrick et al. 1997; Basri & Marcy 1995 and references therein). Recently, Tinney (1997) found cesium absorption lines in spectra of several very low mass stars. This completes the set of alkali metals one would expect to find in such stars.

The reason the alkali metals are important is that they have very low ionization potentials: from 5.390 eV for Li to 3.893 eV for Cs (Letokhov et al. 1987). These are the lowest ionization potentials of any of the elements. As a result, in most stellar atmospheres they are ionized and would only be visible in an ultraviolet spectrum, a wavelength region never used to classify M dwarfs. As one considers stellar atmospheres of cooler and cooler temperatures, the neutral alkalis begin to appear, with Cs appearing only in the very coolest atmospheres. Continuing this progression through cooler atmospheres, as one crosses into the brown dwarf regime, these metals should begin to form molecules. Thus, they would again disappear from the optical to near-IR spectra.

In the case of Gliese 229B, the two strongest cesium lines are present (see Fig. 5). The other alkali metals have their strongest lines blueward of the shortest wavelength we were able to measure. (Li is at 670.8 and 812.6 nm; Na is at 589.5 and 589.0 nm; K is at 769.9 and 766.5 nm, and Rb is at 794.8 and 780.0 nm.) Unfortunately, we are unable to use the lines for a reliable calculation of the abundance of cesium in Gliese 229B because there exist to date no curve-of-growth models for these absorption lines.

The cesium lines present in the optical region of the spectrum of Gliese 229B comprise the principal doublet of cesium. The line at 852.1 nm corresponds to a transition of the solitary valence electron from the $6\ ^2S_{1/2}$ state to the $6\ ^2P_{3/2}$ state. The other line at 894.3 nm corresponds to the transition from $6\ ^2S_{1/2}$ to $6\ ^2P_{1/2}$. (This notation follows the standard spectroscopic notation convention, $^{2S+1}L_J$.) J. D. Kirkpatrick (1997, private communication) has found the same two cesium lines in a new spectrum of GD 165B as well. These are by far the strongest lines of cesium. The next strongest line at 917.2 nm is several times weaker than either of these and is not visible in Gliese 229B.

An important question to answer is: At what temperatures can we expect these alkali metals to form molecules? This question, which requires thermochemical equilibrium calculations, has been thoroughly addressed for planet-sized objects such as Jupiter by Fegley & Lodders (1994). Their thermochemical equilibrium calculations would lead one to believe that none of the alkali metals should be visible in the spectrum of Jupiter, because they ought to have formed molecules already. Indeed, in Jupiter one expects CsCl to dominate over Cs even at temperatures as high as 2000 K. (The brightness temperature in the region of the Cs lines in Gliese 229B is approximately 1300 K.) However, it is not entirely correct to use the calculations for Jupiter when discussing Gliese 229B. The adiabat for Gliese 229B places a given temperature at a substantially lower pressure. A. Burrows (1998, private communication) believes that the turnover from Cs to CsCl in Gliese 229B happens around 1500 K. However, until the full calculations are carried out, reconciling the theory with this detection of atomic Cs cannot happen. It is possible that one merely expects the deep Cs lines we see, but if they are not compatible with thermochemical equilibrium, it is possible that some quantity of Cs is being convected into the observable atmosphere in much the same way as the CO, as we described in § 6. The thermochemical equilibrium calculations could also lead to an important temperature diagnostic for brown dwarfs and very low mass stars. By observing which alkali metals exist in atomic form, one could determine the temperature of a given object through comparison with the thermochemical equilibrium calculations.

These considerations also have implications for the so-called lithium test for brown dwarfs. It may be that the lithium test, in which one attempts to detect atomic lithium in the candidate brown dwarf (Rebolo, Martínez, & Magazzù 1992; Magazzù, Martínez, & Rebolo 1993), might only be meaningful for the highest temperature brown dwarfs. The temperature at which lithium becomes LiOH determines this. For the case of the Jupiter adiabat, this is well above 2000 K (Fegley & Lodders 1994). The field would benefit from new thermochemical equilibrium calculations using the adiabats found for Gliese 229B (Marley et al. 1996; Burrows et al. 1997).

The authors would like to thank Hugh Jones and Davy Kirkpatrick for supplying their data for the purposes of comparison with Gliese 229B. We would also like to thank Davy Kirkpatrick for lengthy discussions on atomic and molecular identifications, Mark Marley for helping with Figure 8 and for excellent discussions of convection and weather, Bruce Fegley for a very thorough referee's report, and Neill Reid for a very useful and thorough reading of the manuscript. S. R. K. graciously thanks the NSF and NASA for support. This work is based on observations obtained at the W. M. Keck Observatory, which is operated jointly by the University of California and the California Institute of Technology. The Munich Image Data Analysis System is developed and maintained by the European Southern Observatory. Finally, we thank Gustav Kirchhoff and Robert Bunsen for discovering cesium.

REFERENCES

Allard, F., & Hauschildt, P. H. 1995, ApJ, 445, 433
Allard, F., Hauschildt, P. H., Baraffe, I., & Chabrier, G. 1996, ApJ, 465, L123
Basri, G., & Marcy, G. W. 1995, AJ, 109, 762
Berriman, G. B., & Reid, I. N. 1987, MNRAS, 227, 315
Burrows, A., Marley, M., Hubbard, W. B., Lunine, J. I., Guillot, T., Saumon, D., Freedman, R., Sudarsky, D., & Sharp, C. 1997, ApJ, 491, 856
Burrows, A., et al. 1996, Nucl. Phys. B Suppl., 51, 76
Butler, R. P., Marcy, G. W., Williams, E., Hauser, H., & Shirts, P. 1997, ApJ, 474, L115
Drossart, P., Encrenaz, T., Schulz, R., & Stüwe, J. A. 1996, Icarus, 121, 199
Fegley, B., Jr., & Lodders, K. 1994, Icarus, 110, 117
———. 1996, ApJ, 472, L37
Geballe, T. R., Kulkarni, S. R., Woodward, C. E., & Sloan, G. C. 1996, ApJ, 467, L101

Golimowski, D. A., Kulkarni, S. R., Burrows, C. J., Brukardt, R. A., & Oppenheimer, B. R. 1998, AJ, submitted
Guillot, T., Gautier, D., Chabrier, G., & Mosser, B. 1994, Icarus, 112, 337
Horne, K. 1986, PASP, 98, 609
Jones, H. R. A., Longmore, A. J., Jameson, R. F., & Mountain, C. M. 1994, MNRAS, 267, 413
Jones, H. R. A., & Tsuji, T. 1997, ApJ, 48, L39
Karkoschka, E. 1994, Icarus, 111, 174
Kirkpatrick, J. D., Henry, T. J., & Irwin, M. J. 1997, AJ, 113, 1421
Kirkpatrick, J. D., Henry, T. J., & McCarthy, D. W. 1991, ApJS, 77, 417
Letokhov, V. S., Andreev, S. V., & Mishin, V. I. 1987, Phys. Rev. Lett., 59, 1274
Magazzù, A., Martín, E. L., & Rebolo, R. 1993, ApJ, 404, L17
Marley, M. S. 1997, in ASP Conf. Ser., Extrasolar Planets and Brown Dwarfs, ed. R. Rebolo (San Francisco: ASP), in press
Marley, M. S., Saumon, D., Guillot, T., Freedman, R. S., Hubbard, W. B., Burrows, A., & Lunine, J. I. 1996, Science, 272, 1919
Massey, P., & Gronwal, C. 1990, ApJ, 358, 344
Matthews, K., Nakajima, T., Kulkarni, S. R., & Oppenheimer, B. R. 1996, AJ, 112, 1678
Matthews, K., & Soifer, B. T. 1994, in Infrared Astronomy with Arrays: The Next Generation, ed. I. McLean (Dordrecht: Kluwer), 239
Mayor, M., & Queloz, D. 1997, Nature, 378, 355
Meadows, V. S., & Crisp, D. 1996, J. Geophys. Res., 101, 4595
Mould, J. R. 1978, ApJ, 226, 923
Nakajima, T., Oppenheimer, B. R., Kulkarni, S. R., Golimowski, D. A., Matthews, K., & Durrance, S. T. 1995, Nature, 378, 464
Noll, K. S. 1993, in ASP Conf. Ser. 41, Astronomical Infrared Spectroscopy, ed. S. Kwok (San Francisco: ASP), 29
Noll, K. S., Geballe, T. R., & Marley, M. 1997, ApJ, 489, L87 (NGM)
Oke, J. B., et al. 1995, PASP, 107, 375
Oppenheimer, B. R., Kulkarni, S. R., Matthews, K., & Nakajima, T. 1995, Science, 270, 1478
Osterbrock, D. E., Fulbright, J. P., & Bida, T. A. 1997, PASP, 109, 614
Rebolo, R., Martín, E. L., & Magazzù, A. 1992, ApJ, 389, L83
Rossow, W. B. 1978, Icarus, 36, 1
Saumon, D., Marley, M. S., Guillot, T., & Freedman, R. S. 1996, BAAS, 28, 1114
Schiavon, R. P., Barbuy, B., & Singh, P. D. 1997, ApJ, 484, 499
Sharp, C. M., & Huebner, W. F. 1990, ApJS, 72, 417
Tinney, C. G. 1997, in ASP Conf. Ser., Extrasolar Planets and Brown Dwarfs, ed. R. Rebolo (San Francisco: ASP), in press
Tinney, C. G., Mould, J. R., & Reid, I. N. 1993, AJ, 105, 1045
Tsuji, T., Ohnaka, K., & Aoki, W. 1996a, A&A, 305, L1
Tsuji, T., Ohnaka, K., Aoki, W., & Nakajima, T. 1996b, A&A, 308, L29
Wolszczan, A., & Frail, D. A. 1992, Nature, 355, 145